frontiers | Frontiers in Physics

TYPE Mini Review
PUBLISHED 13 May 2024
DOI 10.3389/fphy.2024.1356572

OPEN ACCESS

EDITED BY
Paulo Magalhaes Martins,
University of Lisbon, Portugal

REVIEWED BY
Jerimy Polf,
University of Maryland, United States

*CORRESPONDENCE
Chul Hee Min,
chmin@yonsei.ac.kr

RECEIVED 15 December 2023
ACCEPTED 15 April 2024
PUBLISHED 13 May 2024

CITATION
Cheon B-W and Min CH (2024), Prompt gamma imaging system in particle therapy: a mini-review.
Front. Phys. 12:1356572.
doi: 10.3389/fphy.2024.1356572

Prompt gamma imaging system in particle therapy: a mini-review

Bo-Wi Cheon and Chul Hee Min*

Department of Radiation Convergence Engineering, Yonsei University, Wonju, Republic of Korea

Accurate *in-vivo* verification of beam range and dose distribution is crucial for the safety and effectiveness of particle therapy. Prompt gamma (PG) imaging, as a method for real-time verification, has gained prominence in this area. Currently, several PG imaging systems are under development, including gamma electron vertex imaging (GEVI), the Compton camera, the slit camera, and the multi-array type collimator camera. However, challenges persist in dose prediction accuracy, largely due to patient positioning uncertainty and anatomical changes. Although each system demonstrates potential in verifying PG range, further improvements in detection efficiency, spatial resolution, background reduction, and integration into clinical workflows are essential.

KEYWORDS

prompt gamma imaging, particle therapy, imaging system, *in-vivo* dose verification, real-time

1 Introduction

Advancements in radiotherapy have significantly enhanced its effectiveness in tumor control. Particle therapy, a cutting-edge modality, distinguishes itself from conventional X-ray-based radiation therapy by utilizing accelerated ion beams, such as protons or carbon ions. These ion beams, unlike X-rays, exhibit a distinct dose distribution known as the Bragg peak [1]. In the entrance region of the target matter, ions deposit a minimal dose, which gradually increases, reaching a peak due to the Coulomb interactions with electrons in the target matter [2, 3]. The stopping power of these ions incrementally increases, followed by a rapid dose decrease beyond the Bragg peak. Their high relative stopping power and exceptional trajectory precision afford ions a notable advantage in sparing normal tissue adjacent to the target volume.

Consequently, from 1954 to 2023, over 410,000 patients have undergone particle therapy [4]. Of these, 86% received proton therapy, and the remaining 14% underwent heavy ion therapy, primarily using carbon ions. As of January 2024, there are over 116 proton therapy centers and 15 heavy ion therapy centers in clinical operation globally [5]. Additionally, several countries are planning to establish more particle therapy facilities, aiming to build 28 more proton therapy centers and four heavy ion therapy centers [6].

For tumors at the base of the skull, where sensitive tissues such as the eyes and cranial nerves are located, particle therapy has shown high 5-year survival rates of chondrosarcomas in clinical studies: 81.8% and 91% [7, 8]. While the 5-year survival rate for pancreatic cancer is typically less than 5%, it has increased to 52% with no local recurrence post particle therapy and curative resection, as documented in clinical studies [9–13]. Additionally, particle therapy has been effective for head and neck tumors, including adenocarcinoma, malignant melanoma, and sarcoma, which are often resistant to conventional radiotherapy.

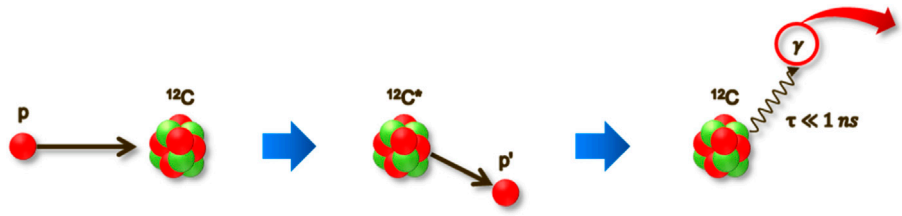

FIGURE 1
Schematic of prompt gamma generation process.

Recent advancements in beam delivery technology, such as intensity-modulated proton therapy pencil beam scanning (IMPT-PBS), have spotlighted particle therapy in oncology with its potential for improved treatment outcomes and more optimistic prognoses compared to conventional radiotherapy [14]. Nonetheless, uncertainties in the treatment process remain, particularly concerning the calibration of ion beam range within tissues using diagnostic X-ray computed tomography (CT) images. Ion radiography and tomography can image patients using the same radiation quality and location as the treatment, aiding in treatment planning [15]. However, inaccuracies in predicting the fall-off region (or beam range) can lead to failure in delivering the planned dose to the target volume or lead to the overdose to adjacent normal tissue [16]. Consequently, developing a methodology to manage beam uncertainty is crucial in particle therapy, given its high sensitivity to factors like patient miss positioning, organ motion, and anatomical changes between treatment sessions.

For *in vivo* beam range verification, Prompt Gamma (PG) detection methods emerged as an alternative, capable of indirectly gauging the range of a particle beam. A variety of methodologies have been introduced such as PG spectroscopy [17–22], PG peak integration [23], coaxial PG monitoring [24], and PG timing [25–30]. In this study, our purpose is to comprehensively focus on the current state of research in PG imaging, which is one of the promising beam range verification methods, and discuss its various applications and the existing limitations that need to be overcome.

2 Prompt gamma imaging

2.1 Principle of prompt gamma imaging

PG imaging is one of the promising methods for *in vivo* beam range verification in particle therapy. PG comprises high-energy photons emitted almost instantaneously (within 1 nanosecond) as a secondary effect of the interaction between high-energy particles (such as protons or carbon ions) and the atomic nuclei within the tissue [31]. The process begins with the accelerated ions colliding with the target nucleus. This collision leads to the nucleus's decay, characterized by the emission of PG as shown in Figure 1. These gammas typically have an energy range from several hundreds of keV to 10 MeV. Reflecting the physical properties of the ion beam—which is characterized by a low entrance dose but delivers a maximum dose in a specific region—PG emissions also start at a lower level when the ion beam initially interacts with the target material. The correlation between the distribution of PG and the depth-dose profile of the particle beam has been observed [31, 32]. The 4.44 MeV energy of PG emitted from tissue-equivalent materials has generally the most similar correlation with the depth-dose distribution, however, each distribution of PG with varying energy peaks exhibits a different correlation [33]. By measuring the PG with a high correlation with the depth-dose profile, the dose profile by the ion beam can be indirectly yet precisely assessed in real-time. Sophisticated imaging systems are therefore imperative in order to effectively acquire PG images in particle therapy.

2.2 Prompt gamma detection modalities

Evaluating the distribution of prompt gamma generally utilizes either electronic or physical collimation methods. Among electronic collimation methods, the Compton camera estimates the initial position by measuring PG scattered by a scatterer, and estimates the incoming gamma direction by measuring the deposited energies and positions of interaction in the detector layers, and then using the Compton equation [34–37], and in the case of Gamma Electron Vertex Imaging (GEVI) [38–40], it estimates the track of PG by using the recoiled electrons through an electron converter. In contrast, slit cameras [41–44] or multi-array collimator cameras [32, 45] are physical collimation methods to physically constrain the gamma trajectory.

2.3 Components of gamma detectors

PG imaging systems generally involve the use of inorganic scintillators as absorber materials, e.g., LYSO, BGO, $LaBr_3$, CsI (TL), and GAGG [46–49]. The scintillator material is selectively used considering the peak wavelength that matches the photo-sensor and the light yield for increased detection efficiency. The collimator generally used high-density materials such as tungsten in physical collimation methods. In the Compton camera for PG imaging, both semiconductors such as cadmium zinc telluride (CZT) and scintillator materials are considered as scatterers and absorbers [34–36]. For photo-sensors, Silicon Photomultiplier (SiPM) or photodiodes are selectively employed. SiPMs, despite their high neutron sensitivity, offer notable advantages like high photon detection efficiency, excellent timing resolution, and

compactness [50]. Photodiodes, on the other hand, exhibit low neutron sensitivity and high linearity with radiation signals. However, the potential influence of temperature sensitivity on the system's stability can be observed in both photo sensors [51].

2.4 Prompt gamma image processing

Although the PG imaging algorithm varies with camera design, one common technique is using energy windows to improve the signal-to-noise ratio in PG imaging [41, 52]. PG imaging with a physical collimator is a technique used to measure the longitudinal distribution of PG emission vertices, which can measure gamma energy or Time-of-Flight (TOF) to enhance the accuracy of range estimation. TOF enables the distinction between PG originating from the target (patient) and gamma produced along the same beamline as the nozzle [53–55]. Effective TOF measurement requires synchronization with the ion beam's nano pulses, which can vary during extraction, often necessitating the use of a fast-beam monitor. In addition, the Maximum Likelihood Expectation Maximization (MLEM) algorithm is also used for image reconstruction in physical collimation methods such as knife-edge or coded aperture [56, 57].

In the PG imaging with electronic collimation systems, such as Compton camera or GEVI, the MLEM algorithm [39, 58, 59] and Stochastic Origin Ensemble (SOE) algorithms [60], for instance, are generally used for image reconstruction in prompt gamma detection. According to a recent study, both reconstruction algorithms showed similar performance. The correlation between the depth-dose range and PG range was within 5 mm in both experimental and simulation scenarios [60, 61]. Recently, there has been a growing interest in exploring an approach that leverages a machine learning-based image reconstruction algorithm to enhance spatial resolution in reconstructed imaging and achieve a close reproduction of the ground truth image in Compton camera [62–64]. The fully connected neural network was generally used to improve the contrast to noise ratio, and average shifts in the beam range as small as 3 mm could be identified.

3 Various imaging systems of prompt gamma in particle therapy

PG imaging systems are generally divided into electronic collimation-based systems, such as GEVI or Compton cameras, and physical collimation-based systems, including knife-edge slit or multi-array type collimator cameras.

3.1 Compton camera and GEVI

The GEVI system operates on the principle of transforming Compton scattered PG into electrons, which are then tracked using a hodoscope [38]. This hodoscope comprises two layers of Double-Sided Silicon Strip Detectors (DSSDs) and a plastic scintillator functioning as a calorimeter. The recently developed GEVI was evaluated for range-shift verification performance in pencil beam scanning proton therapy and was able to detect shifts as small as 1 mm in both global and local shifts. Additionally, shift detection accuracy was also high by measuring global shift within 4 mm error and local shift within 1.9 mm error [40].

The performance of the recently developed Compton camera was evaluated according to various scenarios, such as the energy of the particle beam used in the experiment, the number of primary particles, and reconstruction algorithms. For example, the Polaris-J Compton camera had a difference between the dose range and PG range of about 3 mm at a standard energy of 120 MeV proton beam [60]. MACACO II also confirmed a range difference of about 3 mm in the 150 MeV proton beam [59]. The two-layer dense-pixel Compton camera shows a maximum range difference of about 3 mm, although there is variation depending on the primary particles used in the 150 MeV proton beam [65].

3.2 Knife-edge camera and multi-array collimator camera

The slit camera, utilizing principles of pinhole imaging, measures one-dimensional (1D) PG profiles. This is achieved using a series of gamma detectors aligned behind a knife-edge-shaped slit, designed to capture the PG emissions along the beam path. Through proton beam experiments using pencil beam scanning (PBS) mode, shift search performance can be achieved with a precision of 2 mm by aggregating positions for various spots [66]. Additionally, the first clinical application results of the slit camera, confirmed that the detected PG range is less than 2 mm compared to the average dose range [67].

Conversely, the multi-array collimator camera is designed to measure the two-dimensional (2D) PG distribution. It does this at an angle perpendicular to the beam track, using a parallel-hole collimator within its field of view (FOV). This system was recently tested using 50 MeV protons and was able to provide a two-dimensional distribution of PG. At a standoff distance of 8 cm, a precision of 1 mm (2σ) could be achieved by delivering $(1.7 \pm 0.8) \times 10^8$ protons to the PMMA target, and 1.6 mm (2σ) could be achieved by delivering 5.6×10^{10} protons [68].

3.3 Prompt gamma imaging system with coded-aperture

The coded-aperture approach uses a multi-hole mask for the reconstruction of gamma imaging [69]. Coded-aperture imaging involves encoding and decoding processes. The prompt gamma emission is modulated by the coded-aperture mask and then detected [70]. The decoding procedure reconstructs the image to represent the real position and shape of the object. Uniformly redundant array (URA) and modified uniformly redundant array (MURA) are commonly used apertures in gamma-ray imaging [56]. Correlation analysis is generally used as a reconstruction algorithm that uses the auto-correlation features of coded-aperture arrays. Approaches to confirm dose distribution by measuring PG in 1D or 2D using the coded mask and MLEM image reconstruction algorithm are being considered [57]. In the beam energy range 89.5–107.9 MeV, the average distal fall-off retrieval

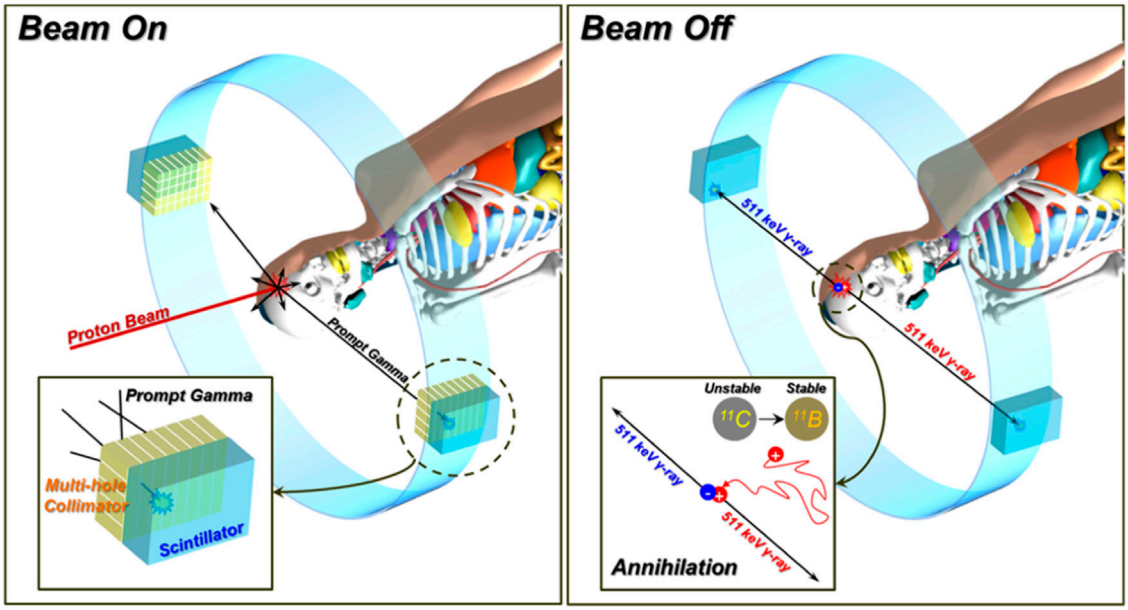

FIGURE 2
The concept of dual-modality type PG imaging system.

precision was 0.72 mm, indicating that the distal fall-off location can be accurately determined.

3.4 Dual-modality type prompt gamma imaging system

Although the range of particle beam can be approximately predicted by imaging the PG distribution and correlating it with the depth-dose profile [31, 32], it is difficult to acquire three-dimensional (3D) distribution. In contrast, PET imaging can provide a 3D dose distribution. On the other hand, the emission distribution depicted by PET shows a comparatively weaker correlation with the actual dose distribution than PG imaging. To harness the strengths of both methods, shown in Figure 2, the concept of a PG and PET combined system was proposed [71–73]. These systems could potentially allow for the acquisition of real-time PG images during the active phase of the beam. Then, once the beam is deactivated, the system could quickly switch to capturing PET images by removing the collimator. Ultimately, the integration of both PG and PET images could enhance the prediction of *in vivo* dose distribution. The performance of one of these systems was experimentally verified with a low-energy proton beam (45 MeV) in the 1 mm difference of PG distribution to depth-dose distribution and the 3 mm difference of positron emitter distribution [72]. On the one hand, hybrid multi-particle approach is also studied to analyze the attributes of each image to establish a formula for forecasting beam range by imaging fast neutrons (FN) and PG generated from nuclear reactions [74]. This research offers the possibility of detecting range shifts at anticipated levels for proton beam intensities in comparing FN and PG imaging. In the simulation setting, range shift detection sensitivities of 1 mm have been successfully attained even at intensities as low as 5×10^8 protons per spot.

3.5 Auto positioning prompt gamma imaging system

A PG camera with a multi-slit imaging system features a collimator with multiple parallel slits paired with an auto-positioning system [75, 76]. The use of multi-slit cameras helps overcome some of the limitations inherent in knife-edge slit cameras. The camera's positioning system is designed to precisely and automatically adjust its location based on the patient's position within the treatment room. The camera head is capable of movement in six degrees of freedom. The Precision Position Tracking (PPT) device is integral to this system. It includes markers placed near the eight vertices of the camera head and a sensor installed in the treatment room. These markers emit infrared light to signal their locations, and the sensor detects these signals to determine the camera's position. This setup allows for real-time adjustment of the camera's position within the treatment room, achieving high accuracy (less than 0.5 mm).

4 Discussion

The evolution of particle therapy marks a significant advancement in radiotherapy, characterized by its precision in targeting tumors and sparing normal tissue. This approach, particularly with the use of ion beams like protons and carbon ions, exploits their unique Bragg peak properties for concentrated dose delivery while minimizing collateral damage. The growing global adoption of particle therapy, evidenced by an increasing

number of treatment centers, highlights its importance in modern oncology. Accurate *in vivo* verification of beam range and dose distribution is crucial to ensuring the safety and efficacy of particle therapy. Nonetheless, the challenge lies in precisely predicting the planned dose, which is sensitive to patient positioning and anatomical changes.

The high-energy PG distribution, a byproduct of particle interactions with tissue, indirectly correlates with the ion beam's depth-dose profile. PG imaging emerges as a promising technique for real-time verification of dose distribution.

There are differences for each PG imaging system, but recently developed PG Imaging systems can resolve under about 2 mm of difference in the low energy (under 50 MeV) proton beam range, and generally about 3 mm beam range searching performance in 120 or 150 MeV proton beam. Most of the findings in these studies were obtained using a homogeneous phantom, the accuracy of predicting beam range varies depending on the number of primary particles. Furthermore, certain findings have not yet been assessed for their suitability in clinical settings, particularly in relation to proton beams below 50 MeV. To ensure the clinical applicability of the PG imaging system, it is additionally required to validate its capability in various conditions (e.g., heterogeneous materials, high energy levels, and low beam intensities).

In addition, the count rate of the current detector device alone may not be sufficient for accurate range monitoring, and improvements in readout electronics and data acquisition systems are required. These key areas for development include improving image resolution, simplifying system complexity, and enhancing real-time data processing. Integrating PG imaging into routine clinical practice necessitates technological advancement, user-friendly interfaces, and streamlined workflows, essential for improving patient outcomes and pushing the boundaries of cancer therapy.

Author contributions

B-WC: Formal Analysis, Investigation, Writing–original draft. CM: Project administration, Writing–original draft, Writing–review and editing.

Funding

The author(s) declare that financial support was received for the research, authorship, and/or publication of this article. This research was supported by National Research Foundation of Korea (NRF); Ministry of Science, ICT, and Future Planning (2020R1A2C2011576), National Research Foundation of Korea (NRF) funded by the Ministry of Science and ICT (RS-2023-00257279), and by the Korea Institute of Energy Technology Evaluation and Planning (KETEP) and the Ministry of Trade, Industry and Energy (MOTIE) of the Republic of Korea (No. 20214000000070).

Conflict of interest

The authors declare that the research was conducted in the absence of any commercial or financial relationships that could be construed as a potential conflict of interest.

Publisher's note

References

1. Wilson RR. Radiological use of fast protons. *Radiology* (1946) 47:487–91. doi:10.1148/47.5.487

2. Knopf AC, Lomax A. *In vivo* proton range verification: a review. *Phys Med Biol* (2013) 58:131–60. doi:10.1088/0031-9155/58/15/R131

3. Schulz RJ, Kagan AR. New technology in radiation oncology. *Oncology* (2004) 18: 249–4. doi:10.2967/jnumed.107.048827

4. Group PTC-O. Particle therapy patient statistics (per end 2023) (update April 2024) (2024). Available from: https://www.ptcog.site/index.php/patient-statistics.

5. Group PTC-O. Particle therapy facilities in clinical operation. (update January 2024) (2024). Available from: https://www.ptcog.site/index.php/facilities-in-operation-public.

6. Group PTC-O. Particle therapy facilities under construction (update January 2024) (2024). Available from: https://www.ptcog.site/index.php/facilities-under-construction.

7. Hug EB, Pelak M, Frank SJ, Fossati P. A review of particle therapy for skull base tumors: modern considerations and future directions. *Int J Part Ther* (2021) 8:168–78. doi:10.14338/IJPT-20-00083

8. Vermorken JB, Budach V, Leemans CR, Machiels JP, Nicolai P, O'Sullivan B. *Critical issues in head and neck oncology: key concepts from the eighth THNO meeting*. Berlin, Germany: Springer International Publishing (2023). doi:10.1007/978-3-031-23175-9

9. Hong TS, Ryan DP, Blaszkowsky LS, Mamon HJ, Kwak EL, Mino-Kenudson M, et al. Phase i study of preoperative short-course chemoradiation with proton beam therapy and capecitabine for resectable pancreatic ductal adenocarcinoma of the head. *Int J Radiat Oncol Biol Phys* (2011) 79:151–7. doi:10.1016/j.ijrobp.2009.10.061

10. Sachsman S, Nichols RC, Morris CG, Zaiden R, Johnson EA, Awad Z, et al. Proton therapy and concomitant capecitabine for non-metastatic unresectable pancreatic adenocarcinoma. *Int J Part Ther* (2014) 1:692–701. doi:10.14338/ijpt.14-00006.1

11. Okada T, Kamada T, Tsuji H, Mizoe JE, Baba M, Kato S, et al. Carbon ion radiotherapy: clinical experiences at national institute of radiological science (NIRS). *J Radiat Res* (2010) 51:355–64. doi:10.1269/jrr.10016

12. Shinoto M, Yamada S, Yasuda S, Imada H, Shioyama Y, Honda H, et al. Phase 1 trial of preoperative, short-course carbon-ion radiotherapy for patients with resectable pancreatic cancer. *Cancer* (2013) 119:45–51. doi:10.1002/cncr.27723

13. Kawashiro S, Yamada S, Okamoto M, Ohno T, Nakano T, Shinoto M, et al. Multi-institutional study of carbon-ion radiotherapy for locally advanced pancreatic cancer: Japan carbon-ion radiation oncology study group (J-CROS) study 1403 pancreas. *Int J Radiat Oncol Biol Phys* (2018) 101:1212–21. doi:10.1016/j.ijrobp.2018.04.057

14. Kabolizadeh P, Ding X, Li X. Advanced particle therapy delivery: a review of advanced techniques for particle therapy delivery. *Princ Pract Part Ther* (2022) 101–13. doi:10.1002/9781119707530.ch7

15. Parodi K, Polf JC. *In vivo* range verification in particle therapy. *Med Phys* (2018) 45:e1036–50. doi:10.1002/mp.12960

16. Albertini F, Hug EB, Lomax AJ. The influence of the optimization starting conditions on the robustness of intensity-modulated proton therapy plans. *Phys Med Biol* (2010) 55:2863–78. doi:10.1088/0031-9155/55/10/005

17. Wang JL, Wu XG, Li ZF, Xie SQ, Hei DQ, Zhao ZH, et al. Prompt gamma spectroscopy retrieval algorithm for element and density measurements accelerated by cloud computing. *Front Phys* (2022) 10. doi:10.3389/fphy.2022.961162

18. Dal Bello R, Magalhaes Martins P, Graça J, Hermann G, Kihm T, Seco J. Results from the experimental evaluation of CeBr3 scintillators for 4He prompt gamma spectroscopy. *Med Phys* (2019) 46:3615–26. doi:10.1002/mp.13594

19. Hueso-González F, Rabe M, Ruggieri TA, Bortfeld T, Verburg JM. A full-scale clinical prototype for proton range verification using prompt gamma-ray spectroscopy. *Phys Med Biol* (2018) 63:185019. doi:10.1088/1361-6560/aad513

20. Tattenberg S, Marants R, Niepel K, Bortfeld T, Sudhyadhom A, Landry G, et al. Validation of prompt gamma-ray spectroscopy for proton range verification in tissue-mimicking and porcine samples. *Phys Med Biol* (2022) 67:205006. doi:10.1088/1361-6560/ac950f

21. Dal BR, Magalhaes Martins P, Brons S, Hermann G, Kihm T, Seimetz M, et al. Prompt gamma spectroscopy for absolute range verification of 12C ions at synchrotron-based facilities. *Phys Med Biol* (2020) 65:095010. doi:10.1088/1361-6560/ab7973

22. Kelleter L, Wrońska A, Besuglow J, Konefał A, Laihem K, Leidner J, et al. Spectroscopic study of prompt-gamma emission for range verification in proton therapy. *Phys Med* (2017) 34:7–17. doi:10.1016/j.ejmp.2017.01.003

23. Krimmer J, Angellier G, Balleyguier L, Dauvergne D, Freud N, Hérault J, et al. A cost-effective monitoring technique in particle therapy via uncollimated prompt gamma peak integration. *Appl Phys Lett* (2017) 110. doi:10.1063/1.4980103

24. Hueso-Gonzalez F, Bortfeld T. Compact method for proton range verification based on coaxial prompt gamma-ray monitoring: a theoretical study. *IEEE Trans Radiat Plasma Med Sci* (2020) 4:170–83. doi:10.1109/TRPMS.2019.2930362

25. Jacquet M, Ansari S, Gallin-Martel ML, André A, Boursier Y, Dupont M, et al. A high sensitivity Cherenkov detector for prompt gamma timing and time imaging. *Sci Rep* (2023) 13:3609–15. doi:10.1038/s41598-023-30712-x

26. Schellhammer SM, Wiedkamp J, Löck S, Kögler T. Multivariate statistical modelling to improve particle treatment verification: implications for prompt gamma-ray timing. *Front Phys* (2022) 10:1–11. doi:10.3389/fphy.2022.932950

27. Pennazio F, Ferrero V, D'Onghia G, Garbolino S, Fiorina E, Marti Villarreal OA, et al. Proton therapy monitoring: spatiotemporal emission reconstruction with prompt gamma timing and implementation with PET detectors. *Phys Med Biol* (2022) 67:065005. doi:10.1088/1361-6560/ac5765

28. Golnik C, Hueso-González F, Müller A, Dendooven P, Enghardt W, Fiedler F, et al. Range assessment in particle therapy based on prompt γ-ray timing measurements. *Phys Med Biol* (2014) 59:5399–422. doi:10.1088/0031-9155/59/18/5399

29. Marcatili S, Collot J, Curtoni S, Dauvergne D, Hostachy JY, Koumeir C, et al. Ultra-fast prompt gamma detection in single proton counting regime for range monitoring in particle therapy. *Phys Med Biol* (2020) 65:245033. doi:10.1088/1361-6560/ab7a6c

30. Jacquet M, Marcatili S, Gallin-Martel ML, Bouly JL, Boursier Y, Dauvergne D, et al. A time-of-flight-based reconstruction for real-time prompt-gamma imaging in proton therapy. *Phys Med Biol* (2021) 66:135003. doi:10.1088/1361-6560/ac03ca

31. Testa E, Bajard M, Chevallier M, Dauvergne D, Le Foulher F, Freud N, et al. Monitoring the Bragg peak location of 73 MeVu carbon ions by means of prompt γ -ray measurements. *Appl Phys Lett* (2008) 93:93. doi:10.1063/1.2975841

32. Min CH, Kim CH, Youn MY, Kim JW. Prompt gamma measurements for locating the dose falloff region in the proton therapy. *Appl Phys Lett* (2006) 89:2–5. doi:10.1063/1.2378561

33. Verburg JM, Riley K, Bortfeld T, Seco J. Energy- and time-resolved detection of prompt gamma-rays for proton range verification. *Phys Med Biol* (2013) 58:L37–49. doi:10.1088/0031-9155/58/20/L37

34. Hosokoshi H, Kataoka J, Mochizuki S, Yoneyama M, Ito S, Kiji H, et al. Development and performance verification of a 3-D position-sensitive Compton camera for imaging MeV gamma rays. *Sci Rep* (2019) 9:18551–9. doi:10.1038/s41598-019-54862-z

35. Kasper J, Rusiecka K, Hetzel R, Kozani MK, Lalik R, Magiera A, et al. The SiFi-CC project – feasibility study of a scintillation-fiber-based Compton camera for proton therapy monitoring. *Phys Med* (2020) 76:317–25. doi:10.1016/j.ejmp.2020.07.013

36. Hart S, Jones P, Pellegri L, Peterson S. A hybrid CZT-LaBr3:Ce Compton camera system for improving proton therapy imaging. *J Phys Conf Ser* (2023) 2586:012130–6. doi:10.1088/1742-6596/2586/1/012130

37. Draeger E, Mackin D, Peterson S, Chen H, Avery S, Polf JC, et al. 3D prompt gamma imaging for proton beam range verification. *Phys Med Biol* (2018) 63. doi:10.1088/1361-6560/aaa203

38. Hyeong Kim C, Hyung Park J, Seo H, Rim Lee H. Gamma electron vertex imaging and application to beam range verification in proton therapy. *Med Phys* (2012) 39:1001–5. doi:10.1118/1.3662890

39. Kim CH, Lee HR, Kim SH, Park JH, Cho S, Jung WG. Gamma electron vertex imaging for *in-vivo* beam-range measurement in proton therapy: experimental results. *Appl Phys Lett* (2018) 113. doi:10.1063/1.5039448

40. Kim SH, Jeong JH, Ku Y, Jung J, Cho S, Jo K, et al. Upgrade of gamma electron vertex imaging system for high-performance range verification in pencil beam scanning proton therapy. *Nucl Eng Technol* (2022) 54:1016–23. doi:10.1016/j.net.2021.09.001

41. Smeets J, Roellinghoff F, Prieels D, Stichelbaut F, Benilov A, Busca P, et al. Prompt gamma imaging with a slit camera for real-time range control in proton therapy. *Phys Med Biol* (2012) 57:3371–405. doi:10.1088/0031-9155/57/11/3371

42. Bom V, Joulaeizadeh L, Beekman F. Real-time prompt gamma monitoring in spot-scanning proton therapy using imaging through a knife-edge-shaped slit. *Phys Med Biol* (2012) 57:297–308. doi:10.1088/0031-9155/57/2/297

43. Perali I, Celani A, Bombelli L, Fiorini C, Camera F, Clementel E, et al. Prompt gamma imaging of proton pencil beams at clinical dose rate. *Phys Med Biol* (2014) 59:5849–71. doi:10.1088/0031-9155/59/19/5849

44. Priegnitz M, Helmbrecht S, Janssens G, Perali I, Smeets J, Vander Stappen F, et al. Detection of mixed-range proton pencil beams with a prompt gamma slit camera. *Phys Med Biol* (2016) 61:855–71. doi:10.1088/0031-9155/61/2/855

45. Sung HK, Jong HP, Youngmo K, Hyun SL, Young-su K, Chan HK, et al. Improvement of Statistics in Proton Beam Range. *J Radiat Prot Res* (2019) 44:1–7. doi:10.14407/jrpr.2019.44.1.1

46. Jan ML, Hsiao IT, Huang HM. Use of a LYSO-based Compton camera for prompt gamma range verification in proton therapy. *Med Phys* (2017) 44:6261–9. doi:10.1002/mp.12626

47. Hueso-Gonzalez F, Pausch G, Petzoldt J, Romer KE, Enghardt W. Prompt gamma rays detected with a BGO block Compton camera reveal range deviations of therapeutic proton beams. *IEEE Trans Radiat Plasma Med Sci* (2017) 1:76–86. doi:10.1109/TNS.2016.2622162

48. Naqvi AA, Al-Matouq FA, Khiari FZ, Isab AA, Rehman KU, Raashid M. Prompt gamma tests of LaBr 3:Ce and BGO detectors for detection of hydrogen, carbon and oxygen in bulk samples. *Nucl Instr Methods Phys Res Sect A Accel Spectrometers, Detect Assoc Equip* (2012) 684:82–7. doi:10.1016/j.nima.2012.05.044

49. Choi HJ, Jang JW, Shin WG, Park H, Incerti S, Min CH. Development of integrated prompt gamma imaging and positron emission tomography system for *in vivo* 3-D dose verification: a Monte Carlo study. *Phys Med Biol* (2020) 65:105005. doi:10.1088/1361-6560/ab857c

50. Dolgoshein B, Balagura V, Buzhan P, Danilov M, Filatov L, Garutti E, et al. Status report on silicon photomultiplier development and its applications. *Nucl Instr Methods Phys Res Sect A Accel Spectrometers, Detect Assoc Equip* (2006) 563:368–76. doi:10.1016/j.nima.2006.02.193

51. Charlton DG, Dowell JD, Homer RJ, Jovanovic P, Kenyon IR, Mahout G, et al. Radiation hardness and lifetime studies of photodiodes for the optical readout of the ATLAS semiconductor tracker. *Nucl Instr Methods Phys Res Sect A Accel Spectrometers, Detect Assoc Equip* (2001) 456:300–9. doi:10.1016/S0168-9002(00)00666-5

52. Min CH, Park JG, An SH, Kim CH. Determination of optimal energy window for measurement of prompt gammas from proton beam by Monte Carlo simulations. *J Nucl Sci Technol* (2008) 45:28–31. doi:10.1080/00223131.2008.10875777

53. Roellinghoff F, Benilov A, Dauvergne D, Dedes G, Freud N, Janssens G, et al. Real-time proton beam range monitoring by means of prompt-gamma detection with a collimated camera. *Phys Med Biol* (2014) 59:1327–38. doi:10.1088/0031-9155/59/5/1327

54. Jacquet M, Marcatili S, Gallin-Martel ML, Bouly JL, Boursier Y, Dauvergne D, et al. A Time-of-flight-based reconstruction for real-time prompt-gamma imaging in protontherapy. *arXiv* (2020) 1–32. doi:10.1088/1361-6560/ac03ca

55. Huang M, Toh Y, Ebihara M, Kimura A, Nakamura S. Development of a correction method for the time-of-flight prompt gamma-ray analysis. *J Appl Phys* (2017) 121. doi:10.1063/1.4978309

56. Zhang R, Gong P, Tang X, Wang P, Zhou C, Zhu X, et al. Reconstruction method for gamma-ray coded-aperture imaging based on convolutional neural network. *Nucl Instr Methods Phys Res Sect A Accel Spectrometers, Detect Assoc Equip* (2019) 934:41–51. doi:10.1016/j.nima.2019.04.055

57. Hetzel R, Urbanevych V, Bolke A, Kasper J, Kercz M, Kołodziej M, et al. Near-field coded-mask technique and its potential for proton therapy monitoring. *Phys Med Biol* (2023) 68:245028. doi:10.1088/1361-6560/ad05b2

58. Koide A, Kataoka J, Masuda T, Mochizuki S, Taya T, Sueoka K, et al. Precision imaging of 4.4 MeV gamma rays using a 3-D position sensitive Compton camera. *Sci Rep* (2018) 8:8116–9. doi:10.1038/s41598-018-26591-2

59. Muñoz E, Ros A, Borja-Lloret M, Barrio J, Dendooven P, Oliver JF, et al. Proton range verification with MACACO II Compton camera enhanced by a neural network for event selection. *Sci Rep* (2021) 11:9325–12. doi:10.1038/s41598-021-88812-5

60. Valencia Lozano I, Dedes G, Peterson S, Mackin D, Zoglauer A, Beddar S, et al. Comparison of reconstructed prompt gamma emissions using maximum likelihood estimation and origin ensemble algorithms for a Compton camera system tailored to proton range monitoring. *Z Med Phys* (2023) 33:124–34. doi:10.1016/j.zemedi.2022.04.005

61. Kohlhase N, Wegener T, Schaar M, Bolke A, Etxebeste A, Sarrut D, et al. Capability of MLEM and OE to detect range shifts with a Compton camera in particle therapy. *IEEE Trans Radiat Plasma Med Sci* (2020) 4:233–42. doi:10.1109/TRPMS.2019.2937675

62. Jiang Z, Polf JC, Barajas CA, Gobbert MK, Ren L. A feasibility study of enhanced prompt gamma imaging for range verification in proton therapy using deep learning. *Phys Med Biol* (2023) 68:075001. doi:10.1088/1361-6560/acbf9a

63. Barajas CA, Polf JC, Gobbert MK. Deep residual fully connected neural network classification of Compton camera based prompt gamma imaging for proton radiotherapy. *Front Phys* (2023) 11:1–11. doi:10.3389/fphy.2023.903929

64. Polf JC, Barajas CA, Peterson SW, Mackin DS, Beddar S, Ren L, et al. Applications of machine learning to improve the clinical viability of Compton camera based *in vivo* range verification in proton radiotherapy. *Front Phys* (2022) 10:838273–13. doi:10.3389/fphy.2022.838273

65. Yao Z, Xiao Y, Dong M, Deng H. Development of a two-layer dense-pixel LYSO Compton camera prototype for prompt gamma imaging. *Phys Med Biol* (2023) 68:045008. doi:10.1088/1361-6560/acb4d8

66. Xie Y, Bentefour EH, Janssens G, Smeets J, Vander Stappen F, Hotoiu L, et al. Prompt gamma imaging for *in vivo* range verification of pencil beam scanning proton therapy. *Int J Radiat Oncol Biol Phys* (2017) 99:210–8. doi:10.1016/j.ijrobp.2017.04.027

67. Richter C, Pausch G, Barczyk S, Priegnitz M, Keitz I, Thiele J, et al. First clinical application of a prompt gamma based *in vivo* proton range verification system. *Radiother Oncol* (2016) 118:232–7. doi:10.1016/j.radonc.2016.01.004

68. Ellin J, Ready J, Negut V, Pak R, Haefner A, Mihailescu L, et al. Evaluation of a novel multi-slit collimated detection system for prompt gamma-ray imaging during proton beam therapy. In: 2018 IEEE Nucl Sci Symp Med Imaging Conf NSS/MIC 2018 - Proc; November, 2018; Sydney, NSW, Australia (2018). p. 1–8.

69. Park S, Hammig MD, Jeong M. Comparison of characteristics of gamma-ray imager based on coded aperture by varying the thickness of the BGO scintillator. *J Radiat Prot Res* (2022) 47:214–225. doi:10.14407/jrpr.2022.00122

70. Goldwurm A, Gros A. *Coded mask instruments for gamma-ray astronomy*. Berlin, Germany: Springer (2023). doi:10.1007/978-981-16-4544-0_44-1

71. Choi HJ, Jang JW, Shin WG, Park H, Incerti S, Min CH. Development of integrated prompt gamma imaging and positron emission tomography system for *in vivo* 3-D dose verification: a Monte Carlo study. *Phys Med Biol* (2020) 65:105005. doi:10.1088/1361-6560/ab857c

72. Cheon BW, Lee HC, You SH, Seo H, Min CH, Choi HJ. Experiment of proof-of-principle on prompt gamma-positron emission tomography (PG-PET) system for *in-vivo* dose distribution verification in proton therapy. *Nucl Eng Technol* (2023) 55:2018–25. doi:10.1016/j.net.2023.03.004

73. Ferrero V, Cerello P, Fiorina E, Monaco V, Rafecas M, Wheadon R, et al. Innovation in online hadrontherapy monitoring: an in-beam PET and prompt-gamma-timing combined device. *Nucl Instr Methods Phys Res Sect A Accel Spectrometers, Detect Assoc Equip* (2019) 936:48–9. doi:10.1016/j.nima.2018.08.065

74. Meric I, Alagoz E, Hysing LB, Kögler T, Lathouwers D, Lionheart WRB, et al. A hybrid multi-particle approach to range assessment-based treatment verification in particle therapy. *Sci Rep* (2023) 13:6709–16. doi:10.1038/s41598-023-33777-w

75. Park JH, Kim SH, Ku Y, Kim CH, Lee HR, Jeong JH, et al. Multi-slit prompt-gamma camera for locating of distal dose falloff in proton therapy. *Nucl Eng Technol* (2019) 51:1406–16. doi:10.1016/j.net.2019.03.008

76. Ku Y, Choi S, Cho J, Jang S, Jeong JH, Kim SH, et al. Tackling range uncertainty in proton therapy: development and evaluation of a new multi-slit prompt-gamma camera (MSPGC) system. *Nucl Eng Technol* (2023) 55:3140–9. doi:10.1016/j.net.2023.05.028